ITALIAN PHYSICAL SOCIETY

PROCEEDINGS

OF THE

INTERNATIONAL SCHOOL OF PHYSICS

«ENRICO FERMI»

COURSE CXIX

edited by G. CASATI, I. GUARNERI and U. SMILANSKY

Directors of the Course

VARENNA ON LAKE COMO

VILLA MONASTERO

23 July - 2 August 1991

Quantum Chaos

1993

NORTH-HOLLAND

AMSTERDAM - OXFORD - NEW YORK - TOKYO

Dynamical Localization in the Hydrogen Atom.

D. L. SHEPELYANSKY

Budker Institute of Nuclear Physics - 630090 Novosibirsk, Russia

1. – Introduction.

During the last years a great number of works were devoted to the creation and investigation of highly excited atoms [1]. In such an atom the electron is moving relatively far from the nucleus and its interaction with other electrons is relatively small. Due to that the properties of any highly excited, or so-called Rydberg, atom in many respects are similar to the properties of the states of the hydrogen atom with large principal quantum number. For these states the radiative lifetime is quite long and, due to large values of the dipole matrix elements, the atom effectively interacts even with small external fields. These properties have allowed the creation of very sensitive detectors of infrared and microwave radiation (see, for example, [2]). Among other applications of Rydberg atoms it is possible to mention their use for the creation of a maser [3], for metrology [4] and astrophysics [5], for isotope separation [6].

The creation of tunable lasers and the development of the atomic-beam technique now allows us to excite atoms in a state with required quantum numbers. The highest principal quantum number achieved in our days in a laboratory experiment is near $n = 500$ [7]. However, the states with the highest values of n have not been created in a laboratory but, as unexpectedly happened, they simply exist in the space plasma [8], so that in the highest states registered there were carbon atoms with $n = 732$ [9]. Such observations allow us to obtain interesting information about space plasma [8-10].

An interesting physical problem is the problem of ionization of highly excited atom in a monochromatic field. This process gives an example of an unusual photoelectric effect for which ionization at a frequency much smaller than the ionization energy ($\hbar\omega \ll I$) goes much faster than for the one-photon frequency [11]. The researches in this field were initiated by the experiment of Bayfield and Koch [12] in which they had observed a strong ionization of an atom with principal quantum number $n \approx 66$ in a linearly polarized microwave field with a field strength $\varepsilon \sim 10$ V/cm and a frequency $\omega/2\pi = 9.9$ GHz. In this

case the value of ε was much less than the value at which ionization takes place in the static electric field, $\varepsilon_{st} = 0.13/n^4$. Also for ionization it was necessary to absorb approximately 100 photons (here and below we use atomic units).

For an explanation of the results of these experiments in [13] a hypothesis about the diffusive mechanism of ionization was suggested. On those grounds the diffusion rate in energy and the estimate for a ionization time were obtained. In ref. [14, 15] the authors, on the basis of the fact that the principal quantum number was $n \gg 1$, applied for the description of ionization the method of numerical solution of the equations of the classical electron motion. As a result they obtained a satisfactory agreement between the ionization probability of the classical atom and its experimental value. The explanation of the appearance of the diffusion and ionization in the classical system was given in [16]. In this paper the authors showed that for a field strength above some critical value the overlapping of the resonances [17] took place and the motion of the electron became chaotic leading to its ionization [16]. It is necessary to stress here that the field is strictly monochromatic and there are no random forces acting on the atom. Further laboratory and numerical experiments were made for different values of the initially excited level n and for different values of the field strength [18, 19]. They showed that the ionization probability obtained in the experiment was close to its classical value and in such a way confirmed the classical picture of the ionization process. These results led the authors of [14-16, 18, 19] to the conclusion that the ionization process, except for some fine details, is perfectly described by classical mechanics and that the quantum effects had ~~an~~ no important influence.

Since the ionization happens due to the appearance of the dynamical chaos in the classical system, the question about the role of quantum effects for an atom in a microwave field is closely related to the fundamental problem of quantum chaos. One of the important directions of research in this new field of physics is the investigation of the excitation of quantum systems by the periodic field. The most interesting effect here is the effect of quantum diffusion limitation which leads to a suppression of classical diffusion excitation by quantum interference. For the first time this phenomenon has been discovered in numerical experiments with the quantum kicked-rotator model [20]. Further investigations have allowed us to understand the reason of the diffusion limitation and to relate the number of effectively excited states with the diffusion rate in the classical system [21-24]. In [25, 26] it was established that in some sense this phenomenon is analogous to the Anderson localization in the solid state. According to this analogy the unperturbed-level number corresponds to the spatial coordinate (site number in the lattice). However, in spite of this analogy it is necessary to stress that the phenomenon of quantum localization of chaos is different from Anderson localization due to the absence of randomness.

The investigations of the simple models of quantum chaos have allowed us to understand the physics of the phenomenon and to apply the results obtained

there for the solution of the problem of microwave ionization of a highly excited atom. It was shown that, in principle, quantum effects play an important role for an arbitrarily large quantum number n and can lead there to the localization of diffusive excitation and to a decrease of the ionization probability in comparison with its classical value [11, 27-33]. However, for a sufficiently strong field and low frequency the localization length in energy, measured by the number of photons, becomes comparable with the number of photons required for ionization. This condition determines the delocalization border above which the quantum excitation is close to the classical one.

The analysis of the experiments [12, 18, 19] shows that one part of them was made for a frequency much shorter than the Kepler frequency. Therefore, the ionization takes place there for a field strength close to the static-field border and does not go in a diffusive way. Another part with a frequency comparable with the Kepler frequency ($\omega_0 = \omega n_0^3 \approx 0.5 \div 1.1$, where n_0 is the initially excited-level number) was in the delocalization region and, therefore, the laboratory results were in agreement with the classical numerical simulations. The understanding of the physics of the quantum localization of the diffusive ionization in the hydrogen atom [11, 27-33] has allowed us to find the conditions at which ionization in the quantum system would be strongly suppressed in comparison with the classical case. Further experiments [34, 35] have confirmed the theoretical predictions and showed that the quantum ionization border is larger than the classical one. Since the diffusive ionization takes place mainly for $\omega_0 > 1$, we will discuss ionization in this region. The analysis of the properties of ionization for $\omega_0 < 1$ can be found in [36]. A recent review of the last experimental and theoretical results is given in [37]. In the following I will present the main results and ideas of the quantum localization theory for the hydrogen atom in a microwave field which have been developed in [11, 27-33, 38-40]. The most detailed derivations of the results are given in [31, 33, 41].

The classical dynamics depends only on the rescaled values of the field strength $\varepsilon_0 = \varepsilon n_0^4$ and frequency $\omega_0 = \omega n_0^3$. For a transition from the atomic units to the physical quantities it is convenient to keep in mind that for $n_0 = 100$ the frequency $\omega/2\pi = 10\,\mathrm{GHz}$ corresponds to $\omega_0 = 1.519\,98$ and the field strength $\varepsilon = 5.144\,85\,\mathrm{V/cm}$ corresponds to $\varepsilon_0 = 0.1$.

2. – Classical dynamics.

We will start the analysis of the classical dynamics from a quite general case when the vector of a linearly polarized field lies in the plane of the electron orbit. Then the Hamiltonian has the form

$$H = \frac{p_x^2}{2} + \frac{p_y^2}{2} - \frac{1}{(x^2 + y^2)^{1/2}} + \varepsilon x \cos \omega t \,, \tag{1}$$

where the field is polarized along x. After the introduction of the action-angle variables for the unperturbed motion this Hamiltonian can be written in the form [16, 33, 41]

$$(2)\quad H = -\frac{1}{2n^2} + \varepsilon n^2 \cos\omega t\left[\cos\psi\left\{\frac{3}{2}e - 2\sum_{s=1}^{\infty} x_s \cos(s\theta)\right\} + \sin\psi\left\{2\sum_{s=1}^{\infty} y_s \sin(s\theta)\right\}\right].$$

Here (n, θ) are the principal quantum number and the conjugated phase, l is the orbital momentum and ψ is the conjugated phase given by the angle between the field and the orientation of the unperturbed ellipse, $e = \sqrt{1 - l^2/n^2}$ is the eccentricity and the coefficients x_s, y_s are given by the Fourier components of $x(t)$ (see [42]):

$$(3)\qquad x_s = \frac{J_s'(se)}{s}, \qquad y_s = \frac{(1-e^2)^{1/2} J_s(se)}{se}.$$

The condition of the resonance has the form $\omega n^3 = s$. For a high frequency $\omega n^3 \approx s \gg 1$ it is convenient to use the following representation for the Bessel function [42]:

$$(4)\quad J_s(se) \approx \frac{1}{\sqrt{\pi}}\left(\frac{2}{s}\right)^{1/3} \Phi\left[\left(\frac{s}{2}\right)^{2/3}(1-e^2)\right] \approx \frac{1}{\sqrt{\pi}}\left(\frac{2}{\omega n^3}\right)^{1/3} \Phi\left[\left(\frac{\omega}{2}\right)^{2/3} l^2\right],$$

where Φ is the Airy function. Since $\Phi(x)$ decays exponentially for $x \gg 1$, the resonant harmonics are negligibly small for the orbital momentum,

$$(5)\qquad l > l_c \approx \left(\frac{2}{\omega}\right)^{1/3},$$

and the motion there is stable. Due to that, in the case when condition (5) is satisfied, ionization can take place only for very strong field when the amplitude of the electron oscillations becomes comparable with the distance between the electron and the atom: $2\varepsilon/\omega^2 > n^2(1-e)$ (see [43] for details). In the case of extended orbits with $e \approx 1$ from (3), (4) we obtain the convenient expression for the resonance amplitudes:

$$(6)\qquad \begin{cases} y_s \approx \dfrac{l}{n}\dfrac{J_s(s)}{s} \approx \dfrac{2^{1/3}}{\sqrt{\pi}}\dfrac{l}{n}\dfrac{\Phi(0)}{s^{4/3}} \approx 0.447\dfrac{l}{n}\dfrac{1}{s^{4/3}}, \\ x_s = \dfrac{1}{s^2}\dfrac{\partial}{\partial e} J_s(se)\Big|_{e=1} \approx -\dfrac{2^{2/3}}{\sqrt{\pi}}\dfrac{\Phi'(0)}{s^{5/3}} \approx \dfrac{0.411}{s^{5/3}}\left(1 + \dfrac{l^2}{2n^2}\right). \end{cases}$$

3. – One-dimensional model.

For the orbits extended along the field direction the dynamics is described by the Hamiltonian of the one-dimensional hydrogen atom

$$H = \frac{p^2}{2} - \frac{1}{x} + \varepsilon x \cos \omega t , \qquad x \geqslant 0, \tag{7}$$

which in action-angle variables has the form

$$H = -\frac{1}{2n^2} + \varepsilon n^2 \cos \omega t \left[\frac{3}{2} - 2 \sum_{s=1}^{\infty} x_s \cos (s\theta) \right]. \tag{8}$$

The resonant values of n are determined from the resonant condition $\omega = s\dot{\theta} = s/n_s^3 = s\Omega_s$. For small field strength near the resonance s we can keep only the resonant term and, after the canonical transformation, we reduce the problem to the Hamiltonian of the pendulum (see details of such approach in [17]),

$$H_s = -\frac{3}{2} \frac{(n - n_s)^2}{n_s^4} - \varepsilon n_s^2 x_s \cos (s\lambda) , \tag{9}$$

where $\lambda = \theta - \omega t/s$ and the first term on the right-hand side is given by the second-order expansion of the unperturbed Hamiltonian. The separatrix curve of (9) corresponds to $H_s = -\varepsilon n_s^2 x_s$. The half-width of the separatrix in action is equal to

$$\Delta n = \left[\frac{4n_s^4}{3} \varepsilon n_s^2 x_s \sin^2 \left(\frac{s\lambda}{2} \right) \right]^{1/2} \Bigg|_{s\lambda = \pi} = \frac{2}{\sqrt{3}} n_s^3 \sqrt{\varepsilon x_s} \tag{10}$$

and its half-width in frequency is

$$\Delta \Omega_s = \frac{3\Delta n}{n_s^4} = \frac{2}{n_s} \sqrt{3\, \varepsilon x_s} . \tag{11}$$

According to the Chirikov criterion of overlapping resonances [17, 44] the motion becomes chaotic after the overlapping of unperturbed resonances. The overlapping parameter is equal to

$$S = (\Delta \Omega_s + \Delta \Omega_{s+1})/(\Omega_s - \Omega_{s+1}) . \tag{12}$$

Since $\Delta \Omega_s \approx \Delta \Omega_{s+1}$ and $\Omega_s - \Omega_{s+1} \approx \omega/s^2$, from (10)-(12) we obtain the condition of global chaos:

$$K = 2.5 S^2 \approx 49 \varepsilon n_s^4 s^{1/3} > 1 , \tag{13}$$

where the empirical numerical factor 2.5 takes into account the effect of the higher-order resonances and the finite width of the chaotic layer [17]. Since K grows with the increase of n, the classical ionization border coincides with the

chaos border [31,33,41]:

$$\varepsilon_0 = \varepsilon n_0^4 > \varepsilon_c = \frac{1}{49\omega_0^{1/3}} . \tag{14}$$

4. – Kepler map.

Another approach to the description of the motion is based on the construction of an approximate canonical map. For the derivation of such a map it is convenient to introduce the «eccentric anomaly» according to

$$\begin{cases} x = n^2(1 - \cos\xi), \\ \omega t = \omega n^3(\xi - \sin\xi) + \phi, \\ \theta = \xi - \sin\xi, \end{cases} \tag{15}$$

where ϕ is the phase of the field at the moment when the electron passes near the nucleus ($\xi = 0$). Then from the Hamiltonian equations and (15) it follows

$$\dot{n} = -\frac{\partial H}{\partial\theta} = -\varepsilon n^2 \cos\omega t \sin\xi \frac{\mathrm{d}\xi}{\mathrm{d}\theta} . \tag{16}$$

Assuming ε to be small, we can use in the right-hand side the unperturbed values of the variables and after the integration over one orbital period of the electron (from aphelion to aphelion with $\xi = \pm\pi$) we get the change of the action:

$$\Delta n = \varepsilon n^5 \sin\phi \int_{-\pi}^{\pi} \sin(\kappa(\xi - \sin\xi)) \sin\xi \,\mathrm{d}\xi = 2\pi\varepsilon n^5 \sin\phi J_\kappa'(\kappa), \tag{17}$$

where $\kappa = \omega n^3$ and $J_\kappa(\kappa)$ is the Anger function. For integer values of κ it coincides with the Bessel function and for $\kappa \gg 1$ it decays as $J_\kappa'(\kappa) \approx 0.41/\kappa^{2/3}$. Therefore, the number of absorbed or emitted photons is equal to $\Delta N = \Delta n/\omega n^3 = \Delta E/\omega = kA(\kappa)\sin\phi$, with $A(\kappa) = \kappa^{2/3} J_\kappa'(\kappa)/0.411$ and $k = 2\pi \cdot 0.411\,\varepsilon/\omega^{5/3}$. Since for $\kappa \gg 1$ the coefficient $A = 1$ (even for $\kappa = 1$ $A \approx 0.8$) we obtain the Kepler map for one orbital period of the electron [30,33,45]:

$$\overline{N} = N + k\sin\phi, \qquad \overline{\phi} = \phi + 2\pi\omega[-2\omega\overline{N}]^{-3/2}, \tag{18}$$

where the second equation gives the change of the field phase during the Kepler period and the bar denotes new values of the variables. The map obtained is the area-preserving map. The change of the energy happens only when the electron passes near the nucleus since there the motion has a singularity. This change takes place during a short interval of time Δt, which is of the order of $1/\kappa$, as is seen from (17). The numerical check of the validity of the map (18) has been

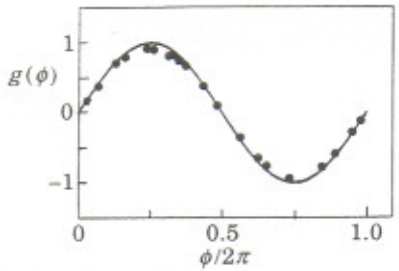

Fig. 1. – Numerically computed function $g(\phi_j)$ (dots) compared to the theoretical curve $\sin\phi$ (full curve) for the case $\varepsilon_0 = \varepsilon n_0^4 = 0.04$, $\omega_0 = \omega n_0^3 = 1.5$.

done in the following way [30, 33]. By the numerical solution of the Hamiltonian equations [7] the phases of the field at the perihelion were computed. Then the check was made by computing $N_j = -[(\phi_j - \phi_{j-1})/2\pi\omega]^{-2/3}/2\omega$, the function $g(\phi_j) = [N_{j+1} - N_j]/k$ and plotting g against ϕ_j (see fig. 1 where a comparison with the theoretical curve $g = \sin\phi$ is also shown). An example of the phase plane for the Kepler map is shown in fig. 2.

To understand the properties of the dynamics of the map (18) it is convenient, following the method of [17], to approximate it locally by the standard map. For that we can linearize the second equation near the resonant (integer) values $\omega(-2\omega N_s)^{-3/2} = s$ and after that we obtain the standard map

$$\overline{N} = N + k\sin\phi, \qquad \overline{\phi} = \phi + T\overline{N} \tag{19}$$

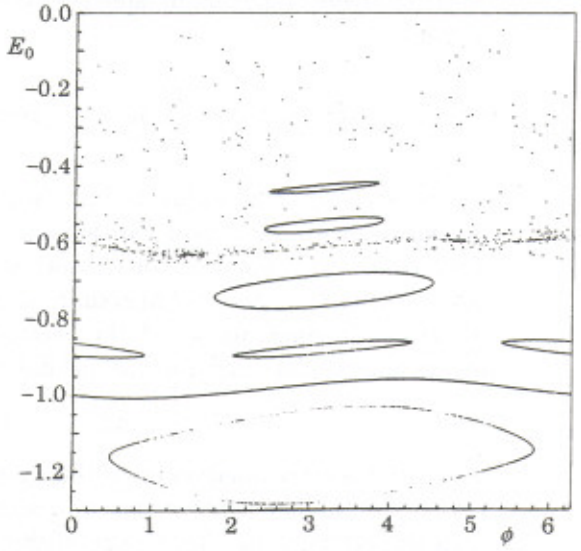

Fig. 2. – Phase space plane for the Kepler map (18) in the variables $E_0 = \omega N n_0^2$, ϕ. Parameter values are $\varepsilon_0 = 0.03$, $\omega_0 = 3.5$. Six regular and one chaotic trajectories are shown.

with $T = \partial(\Delta\phi)/\partial N = 6\pi\omega^2 n^5$. According to [17] the global chaos arises for $K = kT > 1$ that leads to the critical field strength (14) obtained above by another method. Since the value of K grows with n, it is possible to neglect the correlations between the different values of ϕ_j. Then the diffusion rate is given by the random-phase approximation

$$D = \left\langle \frac{(\Delta N)^2}{\Delta t} \right\rangle = \frac{k^2}{2} \approx 3.33 \frac{\varepsilon^2}{\omega^{10/3}}, \tag{20}$$

where the time is measured by the number of orbital periods. The important property of the obtained expression is that the diffusion rate (20) does not depend on n. To estimate the ionization time we need to take into account that the number of photons required for ionization is equal to $N_I = 1/2n_0^2\omega$. Then the ionization time measured by the number of orbital periods is

$$t_I \approx \frac{N_I^2}{D} \approx \frac{\omega_0^{4/3}}{13\,\varepsilon_0^2} \gg 1, \tag{21}$$

where the last inequality gives the condition of applicability of the diffusive description. By recomputing this time by the number of microwave periods τ, we obtain

$$\tau_I \sim \omega_0 t_I \sim \frac{\omega_0^{7/3}}{\varepsilon_0^2}. \tag{22}$$

The excitation process in real time is described by the Fokker-Planck equation for the probability function $f(n)$:

$$\frac{\partial f}{\partial \tau} = \frac{1}{2} \frac{\partial}{\partial n} \left(D_n \frac{\partial f}{\partial n} \right), \tag{23}$$

where the diffusion rate now depends on n:

$$D_n = \left\langle \frac{(\Delta n)^2}{\Delta \tau} \right\rangle = D\omega n^3 = 3.33 \frac{\varepsilon^2}{\omega^{7/3}} n^3. \tag{24}$$

To solve eq. (23) it is convenient to introduce the variables $y = n/n_0$ and $\bar{\tau} = D\tau$. Then the Green function of (23) is equal to

$$G(y\bar{\tau};\, y_0) = \frac{zz_0}{\sqrt{yy_0}} \exp\left[-(z^2 + z_0^2)\right] I_{\pm 2}(2zz_0) \tag{25}$$

with $z = 1/\sqrt{y\bar{\tau}}$, $z_0 = 1/\sqrt{y_0\bar{\tau}}$, $y_0 = 1$. Using the asymptotic behaviour of the

modified Bessel function $I_p = \exp[x]/\sqrt{2\pi x}$, we obtain for $\bar{\tau} \ll 1$, $z \gg 1$ and $\bar{\tau}\sqrt{y} \ll 1$ [31,38]

$$(26)\quad f(y,\bar{\tau}) = \frac{\exp\left[-\left(\frac{1}{\sqrt{y}}-1\right)^2/\bar{\tau}\right] + \exp\left[-\left(\frac{1}{\sqrt{y}}-\frac{2}{\sqrt{\bar{y}}}+1\right)^2/\bar{\tau}\right]}{2y^{3/4}\sqrt{\pi\bar{\tau}}},$$

where the second term takes into account the boundary condition $\partial f/\partial n|_{\bar{n}} = 0$, corresponding to the absence of flux from the chaotic to the regular region $n < \bar{n}$ ($\bar{y} = \bar{n}/n_0$). The obtained solution (26) describes the effective spreading over unperturbed levels with time.

Finally let us note that the Kepler-map description (18) can be applied for $\omega_0 > 1$ and for not a very strong field. The last requirement is satisfied if the change of the energy $k\omega$ after one kick in (18) is larger than the energy of free oscillations of the electron $(\varepsilon/\omega)^2/2$ (see [33, 38]). This gives $\varepsilon < 5\omega^{4/3}$.

5. – Photonic localization.

The numerical solution of the quantum problem shows that quantum effects lead to the suppression of the classical diffusive excitation for some values of the parameters of the system [27,28,31-33]. An example of such a suppression is shown in fig. 3. As is seen, the classical distribution spreads in a diffusive way in agreement with the theoretical prediction (26), while the quantum distribution is localized near the initially excited level. According to the results obtained for the kicked rotator [21,23,24,46] the localization for the steady-state distribution is equal to the diffusion rate (24):

$$(27)\quad l_s \simeq D\Big|_{n=n_0} = 3.33\,\frac{\varepsilon^2}{\omega^{7/3}}\,n^3\Big|_{n=n_0},$$

where l_s gives the localization length in the number of unperturbed levels and the diffusion rate is computed per period of perturbation. If we measure the localization by the number of photons, then from (27) it follows that the localization length is equal to

$$(28)\quad l_{\bar{\tau}} = \frac{l_s}{\omega n^3} = 3.33\,\frac{\varepsilon^2}{\omega^{10/3}} = \frac{k^2}{2} > 1.$$

Since $l_{\bar{\tau}}$ does not depend on n, the quasi-energy eigenstates in average are exponentially localized in energy: $\psi(N) \sim \exp[-|N - N_0|/l_{\bar{\tau}}]$ with $N_0 = -1/2n_0^2\omega$. The obtained expression is applied when $\omega_0 > 1$ and when $l_{\bar{\tau}} > 1$, since in the derivation of relation (28) it was assumed that the diffusion rate is quasi-classically large (see [46]).

Another way of derivation of (28) is the quantization of the Kepler map. In

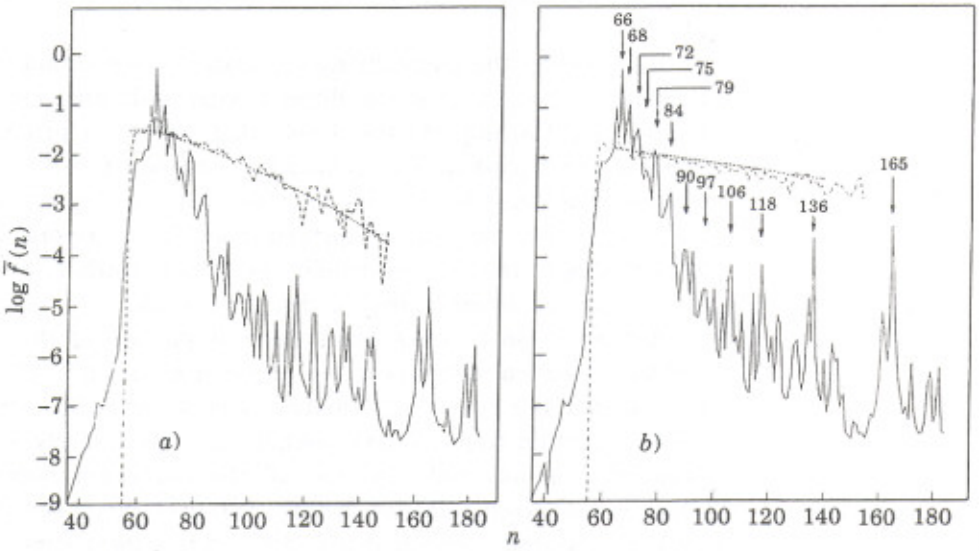

Fig. 3. – Classical (dashed curve) and quantum (solid curve) probability distribution $\bar{f}(n)$ averaged over 40 periods of τ for the case $n_0 = 66$, $\omega_0 = 2.5$, $\varepsilon_0 = 0.04$. In *a*) the average within the interval $80 < \tau < 120$ and in *b*) the average within the interval $560 < \tau < 600$ are given. The dotted lines in both figures represent the analytical solution (26) of the Fokker-Planck equation which fairly agrees with the classical numerical results. The arrows with integers show the positions and the principal quantum numbers of the peaks.

this case $(N, \bar{\phi})$ become operators with the commutation rule $[\hat{N}, \hat{\bar{\phi}}] = -i$ and the map (18) then can be considered as the map for the Heisenberg operators. Due to periodicity of the perturbation in $\bar{\phi}$ the fractional part of N is the integral of motion (like the quasi-momentum). This means that the excitation goes by absorption and emission of an integer number of photons. The Hamiltonian generating the map is

$$H = 2\pi[-2\omega(N_0 + \hat{N}_{\bar{\phi}})]^{-1/2} + k\cos\bar{\phi}\sum_m \delta(t-m), \tag{29}$$

where $0 < \bar{\phi} < 2\pi$, $\hat{N}_{\bar{\phi}} = -i\partial/\partial\bar{\phi}$. It corresponds to some kicked rotator with modified unperturbed spectrum and the period of kicks equal to unity. After integration over the period we obtain the map for the ψ-function:

$$\bar{\psi} = \exp\left[-i\frac{\hat{H}_0}{2}\right]\bar{P}\exp[-ik\cos\phi]\exp\left[-i\frac{\hat{H}_0}{2}\right]\psi, \tag{30}$$

where $\hat{H}_0 = 2\pi[-2\omega(N_0 + \hat{N}_{\bar{\phi}})]^{-1/2}$ is the unperturbed action, $\bar{P}$ is the projection operator on the subspace in which N is negative (the subspace of bounded states $N_{\bar{\phi}} < N_I$), *i.e.* on the subspace where $\exp[-iH_0]$ is defined. Locally (29) can be reduced to the quantum standard map and, therefore, the localization

length in the number of photons is equal to $l_\varphi = D = k^2/2$ in agreement with (28).

By iterating the quantum Kepler map (30) we obtain the distribution in the number of photons. This is a different kind of distribution than the usual distribution over the unperturbed levels that would be produced by iterating the Schrödinger equation. The connection between the two types of distribution can be established by noticing that the photonic transitions generate peaks in the distribution over the unperturbed levels. Therefore, a given photon state corresponds to the total probability in all unperturbed levels lying within a single one-photon interval around the given peak.

A comparison between the numerical solution of the Schrödinger equation and the numerical iteration of the quantum Kepler map (30) is shown in fig. 4. It is seen that the peaked distribution over unperturbed levels is well described by the quantum Kepler map especially near the initially excited level where the probability is maximal. On the tail the agreement persits only in average, which is connected with two factors. The first one is that the Kepler map is an approximate description and it is difficult to expect agreement for exponentially small probability far on the tail. The second reason is connected with the more serious problem of different physical time intervals of the orbital period at different energies. We will return to the discussion of this problem later.

In order to check the theoretical prediction for the localization length (28), the whole range of N_φ was divided into one-photon intervals and in each interval the maximum of the distribution was taken. The numerical value of the localization length was then found as the slope of a straight line fitting the obtained points (for $N_\varphi > 0$). The agreement between the numerical results and the theoretical expression has been checked in an interval of ten orders of magnitude of field intensity for $l_\varphi > 1$ (see fig. 5).

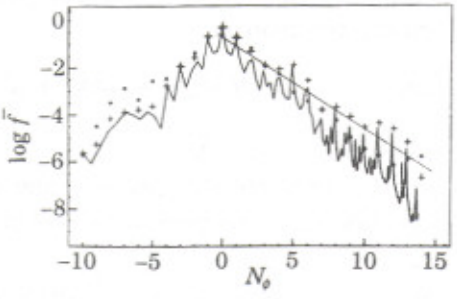

Fig. 4. – The distribution, averaged from 80 to 120 periods of the external field, *vs.* the number of photons $N_\varphi = N_1 - 1/2n^2\omega$. Here $n_0 = 100$, $\varepsilon = 0.04, \omega_0 = 3$. For each integer value of N_φ crosses (+) indicate the probability in the interval $N_\varphi - 1/2$, $N_\varphi + 1/2$. The straight line is the result of a least-square fit. Points were obtained by iterating the quantum map (30).

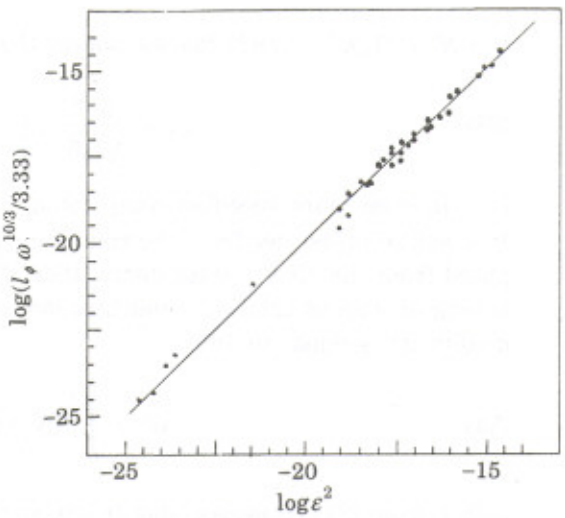

Fig. 5. – Plot of the logarithm of the rescaled experimental localization length $\log(l_\varphi \omega^{10/3}/3.33)$ *vs.* $\log \varepsilon^2$. The solid line is the theoretical dependence from formula (28).

6. – Delocalization.

In the case when the localization length is $l_\varphi \ll N_\varphi$, the steady-state distribution of probabilities is exponentially localized in photon number N_φ and, on the grounds of the analogy with the quantum standard map, we can write the distribution in the form

$$(31) \qquad \bar{f}(N_\varphi) = \frac{1}{2l_\varphi}\left(1 + 2\frac{|N_\varphi|}{l_\varphi}\right)\exp\left[-2\frac{|N_\varphi|}{l_\varphi}\right], \qquad N_\varphi = \frac{1}{2\omega n_0^2} - \frac{1}{2\omega n^2}.$$

Due to the localization the ionization probability in the quantum case is much less than in the classical system. However, for $l_\varphi > N_I$ the localization is destroyed and strong ionization takes place. From this condition we derive the expression for the delocalization border

$$(32) \qquad \varepsilon_0 > \varepsilon_q = \frac{\omega_0^{7/6}}{\sqrt{6.6\, n_0}} = \frac{\omega^{1/6}}{\sqrt{6.6}}\omega_0$$

above which the excitation is close to the classical diffusive process.

For a comparison with the laboratory experiments [34,35] it is necessary to take into account that there the ionization probability was defined as a probability of excitation above some unperturbed level n_c. Then from the condition

$l_{\phi} > N_c = (1/n_0^2 - 1/n_c^2)/2\omega$ we obtain the modified delocalization border

$$\varepsilon_{qc} = \frac{\omega^{1/6}}{\sqrt{6.6}}\omega_0\left(1 - \frac{n_0^2}{n_c^2}\right)^{1/2}. \tag{33}$$

For an even more specified comparison with the experiment we can define the 10% ionization border from the condition that the ionization probability W_I computed from the steady-state distribution (this assumes that the interaction time is long enough to achieve it and that ionization is sufficiently weak and does not modify it) is equal to 10%:

$$W_I = \int_{N_c}^{\infty} \bar{f}(N_{\phi})\,dN_{\phi} = 0.1 \tag{34}$$

with $\bar{f}$ from (31). However, due to the sharp exponential dependence of $\bar{f}$ on N_{ϕ} this leads only to a slight modification of the numerical factor in (34):

$$\varepsilon_{qc} = \frac{\omega^{1/6}}{\sqrt{8}}\omega_0\left(1 - \frac{n_0^2}{n_c^2}\right)^{1/2} \tag{35}$$

showing that the 10% border is not very sensitive to the type of steady-state distribution. Also we need to keep in mind that the theoretical expression gives only the average behaviour for the 10% border and that it can be applied only when $l_{\phi} > 1$.

The comparison of the border (35) with the experimental results [34, 35] shows the satisfactory agreement between both. However, a much better agreement takes place if we compare the experimental data [34] with the results for the 10% border obtained from the numerical simulation of the quantum Kepler map [39] (fig. 6). This comparison shows that the quantum Kepler map reproduces in a quite good way even the fluctuations observed in the experiment and gives one more confirmation that this map describes the real physical process of excitation. On the basis of the mapping of the dynamical problem on a solid-state model (see [24-26, 39]), we may conclude that these fluctuations are analogous to the mesoscopic fluctuations of the conductance in the solid state (W_I is proportional to a current) [39].

It is interesting to compare the rate of ionization in the delocalized region with the one-photon ionization rate [11, 31]. According to (22) for $\omega_0 = 1$ this rate is equal to $\gamma_D \sim \varepsilon_0^2$ (ionization rate per orbital period). For the same field strength the one-photon ionization rate ($\omega_0 = n_0/2$) is equal to $\gamma_1 = (k/2)^2/\omega_0 \sim \varepsilon_0^2/n_0^{7/3}$. From this relation we obtain that the diffusive ionization rate is much larger than the direct one-photon ionization:

$$\frac{\Gamma_D}{\Gamma_1} = \frac{\gamma_D}{\omega_0\gamma_1} \sim n_0^{4/3}. \tag{36}$$

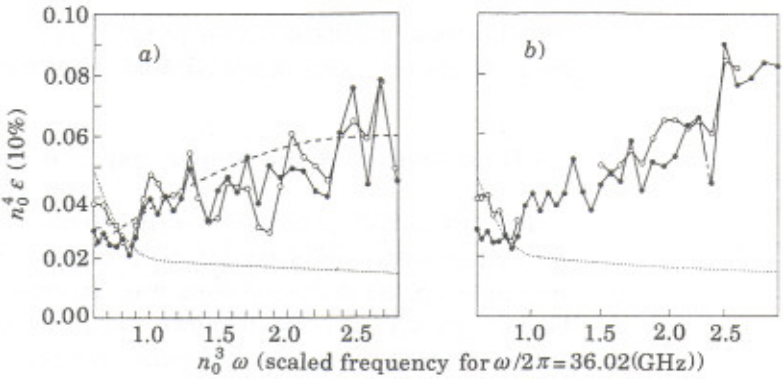

Fig. 6. – Scaled 10% threshold fields from experimental results (taken from fig. 2*a* of ref. [34], $\omega/2\pi = 36.02$ GHz, circles) and from numerical integration of the quantum Kepler map (full circles) [39]. Curves have been drawn to guide the eye. The dashed line is the quantum delocalization border (35). The dotted curve is the classical chaos border. The cases of two different cut-offs are shown ($n_c = 90\,(a)$), $n_c = 175\,(b)$)).

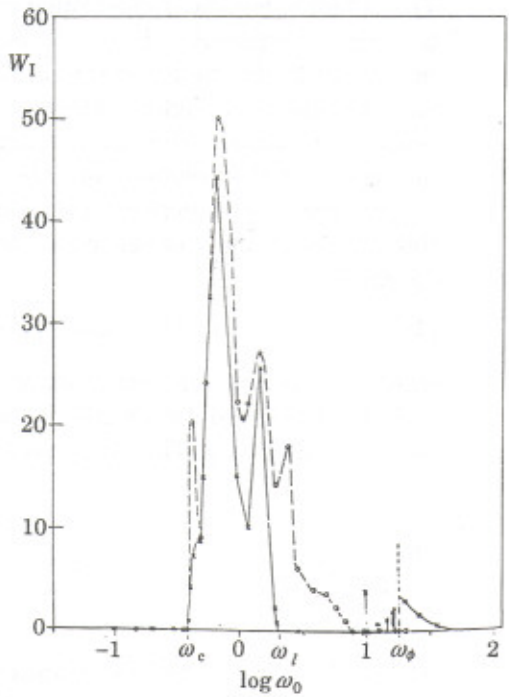

Fig. 7. – Ionization probability $W_I = \sum_{n > n_c} f(n)$ *vs.* field frequency ω_0 after a time $\tau = 40\omega_0$ which corresponds to the same physical time t for all frequencies, $n_0 = 66$, $\varepsilon_0 = 0.05$, $n_c = 99$. Classical numerical results are given by the dashed line, quantum results are given by the full line.

The numerical results obtained from the solution of the Schrödinger equation are in agreement with this analytical prediction (fig. 7).

7. – Quantization of the Kepler map and the scattering problem.

The problem of quantization of the Kepler map is connected with the different physical time scales for orbital periods with different energies. This problem can be solved in the following way. In expressions (29), (30) we can consider the quantity ωN_0 as some unknown quasi-energy E, which is the constant of the motion. Then the map for $\bar{\psi}$ after one orbital period will give the new quantity $\bar{\bar{\psi}}$ which must be equal to $\bar{\psi}$ since the motion over the orbit is a cyclic motion. This leads to the quantization condition [38]

$$\bar{\bar{\psi}} = \exp\left[-i\pi[-2E - 2\omega\hat{N}_{\bar{\varphi}}]^{-1/2}\right]\bar{P}\cdot$$

$$\cdot \exp[-ik\cos\bar{\varphi}]\exp[-i\pi[-2E - 2\omega\hat{N}_{\bar{\varphi}}]^{-1/2}]\bar{\psi} = U_-\bar{\psi} = \bar{\psi}. \tag{37}$$

The obtained nonlinear eigenvalue equation allows one in principle to determine the quasi-energies $E = E_r - i\Gamma/2$ which will have a real (E_r) and an imaginary part ($-i\Gamma/2$) due to absorption in the continuum. The same equation for quasi-energies but in a slightly different form was derived in [47], however the absence of the physical picture of the process did not allow one to understand the properties of the solutions of (37).

Another way of deriving (37) can be found from the scattering problem. In this approach one passage near the nucleus is given by the unitary evolution operator

$$U = \exp[i\partial_N]\exp[-ik\cos\bar{\varphi}]\exp[i\partial_N], \tag{38}$$

where ∂_N are the scattering phases for electrons with positive energies $E_N = E + \omega N > 0$ and for negative energies $E_N < 0$ they are classical actions ($\partial_N = -\pi(-2E_N)^{-1/2}$). Then the evolution operator can be presented in the form

$$U = \left(\begin{array}{c|c} U_+ & R_+ \\ \hline R_- & U_- \end{array}\right), \tag{39}$$

where U_+ and U_- give the transitions in the continuum and discrete parts of the spectrum and R_- and R_+ give the transitions from the continuum to the discrete part of the spectrum and back correspondingly. Then the scattering matrix can be written in the form

$$S = U_+ + R_+(1 + U_- + U_-^2 + U_-^3 + \ldots)R_- = U_+ + R_+\frac{1}{1 - U_-}R_-, \tag{40}$$

where the summation over all powers of U_- comes from the sum of all passages near the nucleus in the discrete part of the spectrum. The equation for the poles of the S-matrix determines the complex quasi-energies and coincides with eq. (37). It is possible to show that the unitarity of the matrix U (38) involves the unitarity of the S-matrix (40).

It is also interesting to make an estimate for the absorption cross-section in the scattering of an electron on an atom in the presence of a microwave field. For that we need to know the properties of the dynamics in the 3-dimensional case. The analytical and numerical analysis carried out in [31, 33] has shown that, due to the degeneracy of the hydrogen spectrum, the excitation in energy for $l < l_c$ (5) still could be described by the Kepler map with the constant k multiplied by some $H < 1$ slightly dependent on (l, ψ). Therefore, roughly a half of the electrons with $l < l_c$ will be captured after a passage near the nucleus if their energy $E < k\omega$. On those grounds we obtain the estimate for the absorption cross-section:

$$\sigma_a \sim \pi\rho^2 \sim \pi \frac{l_c^2}{p^2} \sim \frac{1}{\omega^{2/3} E} . \tag{41}$$

For $E \sim k\omega$ we obtain that the absorption cross-section is quite large: $\sigma_a \sim 1/\varepsilon \sim 10^{-7}\,\mathrm{cm}^2$ for $\varepsilon = 10$ V/cm.

9. – Conclusion.

Using the ideas and the physical understanding of the kicked-rotator model we were able to understand the process of ionization of a highly excited hydrogen atom in a microwave field. Unexpectedly this system happened to be connected with many lines of modern development in physics including Anderson localization, quantum and classical chaos. Only few experiments [34, 35] have been made in the localization regime, actually they only started to feel the suppression of chaos, and it will be quite interesting to carry out experiments in a deeper localized regime. Another interesting line of research is being developed in the Munich group of Prof. H. WALTHER with microwave ionization of Rydberg atoms. There arises the question about the classical simulation of atoms with quantum defect. There is also an interesting question about the destruction of the Coulomb degeneracy that can lead to the 2-dimensional localization problem (a more detailed discussion of the properties of 3-dimensional atoms in a microwave field is given in [33]). The open problem is the statistics of the ionization rates Γ_n in the chaotic regime. A first step in this direction was made in [48] by the investigation of the ionization rates in the kicked-rotator model with absorption.

At the end we present the picture of the ionization borders (fig. 8 [38]). For $\omega_0 > 1$ there are the chaos border (14) and the quantum stability border $k < 1$

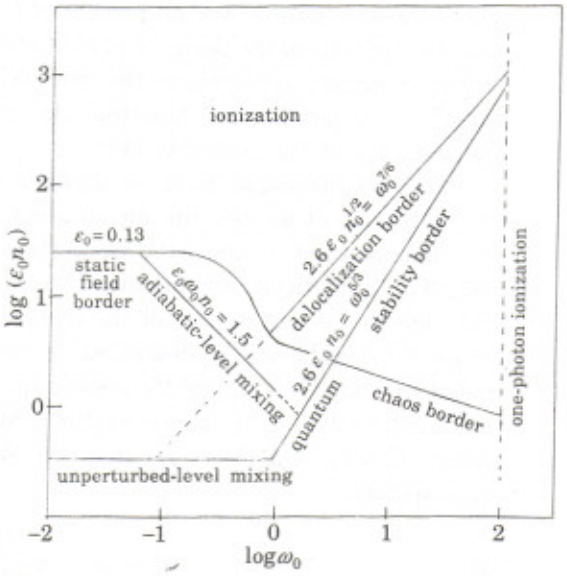

Fig. 8. – Ionization borders for $n_0 = 200$.

below which the probability of one-photon transition is small. The last one is in fact the Shuryak border of chaos [49] below which chaos is suppressed by the quantum perturbation theory. The highest and, therefore, the most important is the delocalization border (32). For $\omega_0 < 1$ the highest is the static-field border. For the hydrogen atom there is also the border of mixing of adiabatic levels ($\varepsilon_0 \omega_0 n_0 = 1.5$) below which the probability remains on the adiabatic Stark level corresponding to the instant field strength. This border in fact was for the first time discussed in [36]. However, for alkali atoms the possibility of the crossing of levels with different orbital momenta leads to a sharp decrease of the ionization border for $\omega_0 \ll 1$ ($3\varepsilon_0 n_0 = 1$) [50].

REFERENCES

[1] *Rydberg States of Atoms and Molecules*, edited by R. F. STEBBINGS and F. B. DUNNING (Cambridge University Press, Cambridge, 1983).
[2] P. FILIPOVICZ, P. MEYSTRE, G. REMPE and H. WALTHER: *Opt. Acta*, **32**, 1105 (1985).
[3] D. MESCHEDE and H. WALTHER: *Phys. Rev. Lett.*, **54**, 551 (1985).
[4] J. LIANG, M. GROSS, P. GOY and S. HAROCHE: *Phys. Rev. A*, **33**, 4437 (1987).
[5] A. DALGARNO: in *Rydberg States of Atoms and Molecules*, edited by R. F. STEBBINGS and F. B. DUNNING (Cambridge University Press, Cambridge, 1983), p. 1.
[6] V. C. LETOKHOV: *Usp. Fiz. Nauk*, **153**, 311 (1989).

[7] J. NEUKAMMER, H. RINNEBERG, K. VIETZKE, A. KONIG, H. HIERONYMUS, M. KOHL, H.-J. GRABKA and G. WUNNER: *Phys. Rev. Lett.*, **59**, 2947 (1987).
[8] R. L. SOROCHENKO and A. E. SOLOMONOVICH: *Priroda*, No. **11**, 82 (1987).
[9] A. A. KONOVALENKO: *Pis'ma Astron. Ž.*, **10**, 846 (1984).
[10] A. A. KONOVALENKO: *Pis'ma Astron. Ž.*, **10**, 912 (1984).
[11] G. CASATI, B. V. CHIRIKOV, I. GUARNERI and D. L. SHEPELYANSKY: *Phys. Rev. Lett.*, **57**, 823 (1986).
[12] J. E. BAYFIELD and P. M. KOCH: *Phys. Rev. Lett.*, **33**, 258 (1974).
[13] N. B. DELONE, B. A. ZON and V. P. KRAINOV: *Ž. Èksp. Teor. Fiz.*, **75**, 445 (1978).
[14] J. D. LEOPOLD and I. C. PERCIVAL: *Phys. Rev. Lett.*, **41**, 944 (1978).
[15] J. D. LEOPOLD and I. C. PERCIVAL: *J. Phys. B*, **12**, 709 (1979).
[16] B. I. MEERSON, E. A. OKS and P. V. SASOROV: *Pis'ma Ž. Èksp. Teor. Fiz.*, **29**, 79 (1979).
[17] B. V. CHIRIKOV: *Phys. Rep.*, **52**, 263 (1979).
[18] K. A. H. VAN LEEUWEN, G. V. OPPEN, S. RENWICK, J. B. BOWLIN, P. M. KOCH, R. V. JENSEN, O. RATH, D. RICHARDS and J. G. LEOPOLD: *Phys. Rev. Lett.*, **55**, 2231 (1985).
[19] P. M. KOCH, K. A. H. VAN LEEUWEN, O. RATH, D. RICHARDS and R. V. JENSEN: *Lecture Notes in Physics*, **278**, 106 (1987).
[20] G. CASATI, B. V. CHIRIKOV, F. M. IZRAILEV and J. FORD: *Lecture Notes in Physics*, **93**, 334 (1979).
[21] B. V. CHIRIKOV, F. M. IZRAILEV and D. L. SHEPELYANSKY: *Sov. Sci. Rev. C*, **2**, 209 (1981); *Physica D*, **33**, 77 (1988).
[22] D. L. SHEPELYANSKY: *Physica D*, **8**, 208 (1983).
[23] B. V. CHIRIKOV and D. L. SHEPELYANSKY: *Radiofizika*, **29**, 1041 (1986).
[24] D. L. SHEPELYANSKY: *Physica D*, **28**, 103 (1987).
[25] S. FISHMAN, D. R. GREMPEL and R. E. PRANGE: *Phys. Rev. Lett.*, **49**, 509 (1982).
[26] S. FISHMAN, D. R. GREMPEL and R. E. PRANGE: *Phys. Rev. A*, **29**, 1639 (1984).
[27] D. L. SHEPELYANSKY: preprint of the Institute of Nuclear Physics 83-61, Novosibirsk (1983); in *Proceedings of the International Conference on Quantum Chaos 1983* (Plenum Press, New York, N.Y., 1985), p. 187.
[28] G. CASATI, B. V. CHIRIKOV and D. L. SHEPELYANSKY: *Phys. Rev. Lett.*, **53**, 2525 (1984).
[29] G. CASATI, B. V. CHIRIKOV, I. GUARNERI and D. L. SHEPELYANSKY: *Phys. Rev. Lett.*, **56**, 2437 (1986).
[30] G. CASATI, I. GUARNERI and D. L. SHEPELYANSKY: *Phys. Rev. A*, **36**, 3501 (1987).
[31] G. CASATI, B. V. CHIRIKOV, I. GUARNERI and D. L. SHEPELYANSKY: *Phys. Rep.*, **154**, 77 (1987).
[32] G. CASATI, B. V. CHIRIKOV, I. GUARNERI and D. L. SHEPELYANSKY: *Phys. Rev. Lett.*, **59**, 2927 (1987).
[33] G. CASATI, I. GUARNERI and D. L. SHEPELYANSKY: *IEEE J. Quantum Electron.*, **24**, 1420 (1988).
[34] E. J. GALVEZ, B. E. SAUER, L. MOORMAN, P. M. KOCH and D. RICHARDS: *Phys. Rev. Lett.*, **61**, 2011 (1988).
[35] J. E. BAYFIELD, G. CASATI, I. GUARNERI and D. W. SOKOL: *Phys. Rev. Lett.*, **63**, 364 (1989).
[36] R. BLUMEL and U. SMILANSKY: *Z. Phys. D*, **6**, 83 (1987).

[37] R. V. JENSEN, S. M. SUSSKIND and M. M. SANDERS: *Phys. Rep.*, **201**, 1 (1991).
[38] D. L. SHEPELYANSKY: *The theory of diffusive photoelectric effect*, preprint of the Institute of Nuclear Physics No. 89-54, 89-89, 89-93, Novosibirsk (1989) (in Russian).
[39] G. CASATI, I. GUARNERI and D. L. SHEPELYANSKY: *Physica A*, **163**, 205 (1990).
[40] G. CASATI and I. GUARNERI: *Comments At. Mol. Phys.*, **25**, 185 (1991).
[41] N. B. DELONE, V. P. KRAINOV and D. L. SHEPELYANSKY: *Usp. Fiz. Nauk*, **140**, 335 (1983) (*Sov. Phys. Usp.*, **26**, 551 (1983)).
[42] L. D. LANDAU and E. M. LIFSHITZ: *Field Theory* (Nauka, Moscow, 1973), sect. 70.
[43] F. BENVENUTO, G. CASATI and D. L. SHEPELYANSKY: *Phys. Rev. A*, **45**, R7670 (1992).
[44] B. V. CHIRIKOV: *At. Energ.*, **6**, 630 (1959).
[45] V. GONTIS and B. KAULAKYS: *J. Phys. B*, **20**, 5051 (1987).
[46] S. FISHMAN: this volume, p. 187.
[47] I. YA. BERSONS: *Ž. Èksp. Teor. Fiz.*, **86**, 860 (1984).
[48] F. BORGONOVI, I. GUARNERI and D. L. SHEPELYANSKY: *Phys. Rev. A*, **43**, 4517 (1991).
[49] E. V. SHURYAK: *Ž. Èksp. Teor. Fiz.*, **71**, 2039 (1976).
[50] P. PILLET, H. B. VAN LINDEN, H. B. VAN DEN HEUVELL, W. W. SMITH, R. KACHRU, N. H. TRAU and T. F. GALLAGHER: *Phys. Rev. A*, **30**, 280 (1984); T. F. GALLAGHER: *Phys. Rev. Lett.*, **61**, 2304 (1988).